

A resonant pair of warm giant planets revealed by *TESS*

David Kipping^{1*}, David Nesvorný², Joel Hartman³, Guillermo Torres⁴,
Gaspar Bakos³, Tiffany Jansen¹, Alex Teachey¹

¹*Dept. of Astronomy, Columbia University, 550 W 120th Street, New York NY 10027, USA*

²*Dept. of Space Studies, Southwest Research Institute, 1050 Walnut Street, Suite 300, Boulder, CO 80302, USA*

³*Dept. of Astrophysical Sciences, Princeton University, NJ 08544, USA*

⁴*Harvard-Smithsonian Center for Astrophysics, 60 Garden Street, Cambridge, MA 02138, USA*

Accepted . Received ; in original form

ABSTRACT

We present the discovery of a pair of transiting giant planets using four sectors of *TESS* photometry. TOI-216 is a $0.87 M_{\odot}$ dwarf orbited by two transitters with radii of $8.2 R_{\oplus}$ and $11.3 R_{\oplus}$, and periods of 17.01 d and 34.57 d, respectively. Anti-correlated TTVs are clearly evident indicating that the transitters orbit the same star and interact via a near 2:1 mean motion resonance. By fitting the TTVs with a dynamical model, we infer masses of $30^{+20}_{-14} M_{\oplus}$ and $200^{+170}_{-100} M_{\oplus}$, establishing that the objects are planetary in nature and have likely sub-Kronian and Kronian densities. TOI-216 lies close to the southern ecliptic pole and thus will be observed by *TESS* throughout the first year, providing an opportunity for continuous dynamical monitoring and considerable refinement of the dynamical masses presented here. TOI-216 closely resembles Kepler-9 in architecture, and we hypothesize that in such systems these Saturn-analogs failed to fully open a gap and thus migrated far deeper into the system before becoming trapped into resonance, which would imply that future detections of new analogs may also have sub-Jupiter masses.

Key words: planets and satellites: detection — stars: individual (TIC 55652896)

1 INTRODUCTION

A small fraction of exoplanets in the cosmos have the correct orbital geometry to transit their star as seen from our home. These transiting planets have been a “royal road to success” in planet discovery (Russell 1948; Winn 2010) yielding thousands of discoveries in recent years (see the NASA Exoplanet Archive; Akeson et al. 2013), despite the fact that they represent just a sliver of the total population. An even more rarefied population is that of transiting planets exhibiting transit timing variations (TTVs; Agol et al. 2005; Holman & Murray 2005; Deck & Agol 2015). For these special worlds, not only can one infer the planetary size from the transit depths, but dynamical modeling of the TTVs can often provide planetary masses too - a fact heavily exploited by *Kepler* (Holman et al. 2010; Lithwick et al. 2012; Nesvorný et al. 2012). In such cases, it is therefore possible to confirm the planetary nature of a system almost exclusively from photometric observations (e.g. Ford et al. 2011; Steffen et al. 2013).

Kepler enjoyed many successes with this strategy, largely enabled by its patience to stare at the same stars for over four years continuously. With *TESS*, the full-sky nature of the survey means that most parts of the sky are observed for much shorter windows¹, potentially posing a challenge to dynamical confirmation of planetary candidates. However, *TESS* does maintain a longer vigil on the ecliptic poles, observing these fields for up to a year continuously (Ricker et al. 2016).

In this work, we describe the discovery of two *TESS* planets near a 2:1 mean motion resonance (MMR) leading to highly significant TTVs. Thanks to the host star’s fortuitous location near the southern ecliptic pole, *TESS* can observe the target for most of the first year making TOI-216 an excellent target for monitoring planet-planet interactions. We describe the observations by *TESS* in Section 2 with attention to detrending, contamination and stellar properties. In Section 3 we regress light curve models and TTV models, demonstrating that the system is a pair of planet-mass objects gravitationally interacting with one another. Finally,

* E-mail: dkippling@astro.columbia.edu

¹ This situation could change if with an extended *TESS* mission (Bouma et al. 2017)

we discuss the possibilities opened up by this exciting new system in Section 4.

2 OBSERVATIONS

2.1 Identification

TIC 55652896 was observed by *TESS* in the first four sectors of year one, and indeed is scheduled to be observed in every sector of that year except for sector 10 (2019-Mar-26 to 2019-Apr-22). Falling on camera 4, the target is a relatively rare example of a transiting planetary system caught within the *TESS* continuous viewing zone (CVZ). With an ecliptic latitude of -82.476408° , we highlight that the target also lands close to JWST’s planned CVZ and would be observable for $\gtrsim 260$ days per year of the mission.

A *TESS* alert was issued on 2018-11-30 for two candidate transiting planets associated with TIC 55652896 using sectors 1 and 2, dubbed TOI-216.01 and TOI-216.02. With periods of ~ 17.1 days (TOI-216.02) and ~ 34.5 days (TOI-216.01), the outer candidate was only seen to transit twice during this time (once per sector).

Amongst the 300+ TOIs identified at the time of writing, this pair stood out as particularly interesting because the planetary candidates lie near a 2:1 period commensurability. If the objects were orbiting the same star, and gravitationally interacting, then it may be possible to confirm the planetary nature of the pair without any ground based follow-up (e.g. see Steffen et al. 2013). For this reason, we decided to further study this system.

2.2 Stellar properties

TOI-216 has an apparent magnitude of 11.5 in the *TESS* bandpass. From the *TESS* Input Catalog (TIC) version 7 (Stassun et al. 2018), catalog survey spectroscopy of the star constrains $T_{\text{eff}} = (5026 \pm 125)$ K, $[M/H] = 0.32 \pm 0.10$ and $\log(g) = 4.66 \pm 0.20$. These properties are used by TIC to infer $M_\star = (0.879 \pm 0.073) M_\odot$ and $R_\star = (0.715 \pm 0.166) R_\odot$.

We also queried the star within *Gaia* DR2 (Gaia Collaboration et al. 2018) and find a parallax measurement of 5.591 ± 0.028 mas (GAIA DR2 4664811297844004352). Rather than use the TIC-7 summary statistics for stellar mass and radius, we would prefer to work with posterior samples - as well as include the *Gaia* parallax - and so we elected to perform our own Bayesian isochrone fitting. To this end, we used the `isochrones` package by T. Morton using the previously listed constraints on V , T_{eff} , $[M/H]$, $\log g$ and parallax with the `Dartmouth` stellar evolution models.

The inputs to our fits (the “star.ini” file) are given in the top panel of Table 1, and the derived parameters of interest in the lower panel. As expected, our results closely agree with those listed in the TIC, although our inference is more precise as a result of using the GAIA parallax which was not available when TIC-7 was compiled.

2.3 Contamination

With a pixel size of 21 arcseconds, there is a greater chance of crowding with *TESS* than *Kepler*. The aperture used in each sector varies slightly but is approximately 4 by 3 pixels

Table 1. Medians and one-sigma uncertainties for the stellar properties of TIC 55652896. The top panel are the properties listed in the TIC version 6 (Stassun et al. 2018), as well as the *Gaia* DR2 parallax. The lower panel lists the derived properties through isochrone matching.

parameter	value
V	12.324 ± 0.069
T_{eff} K	5026 ± 125
$[M/H]$ [dex]	0.32 ± 0.10
$\log g$ [dex]	4.66 ± 0.20
parallax [mas]	5.591 ± 0.028
$M_\star [M_\odot]$	$0.874^{+0.035}_{-0.034}$
$R_\star [R_\odot]$	$0.838^{+0.043}_{-0.030}$
$\rho_\star [\text{kg m}^{-3}]$	2090^{+270}_{-300}
d [pc]	$178.84^{+0.89}_{-0.88}$

and thus sources out to 84 arcseconds can contaminate the aperture.

Fortunately, there are no comparably bright stars that lie within this region. The nearest star listed in the TIC to our target is TIC 55652894, separated by 48.2 arcseconds but far fainter with an apparent *TESS* magnitude of 16.3 (1.2% the brightness level). *Gaia* DR2 (Gaia Collaboration et al. 2018) reports 46 stars within 84 arcseconds, with *G*-band magnitudes from 17.1 to 21.1 (TOI-216 is 12.2). Together, these sources could maximally dilute the target by 5.6% in *G*, although the true value will be less due to color correction to the redder *TESS* bandpass, location of the sources and the finite PSF widths.

These contaminating source cumulatively lead to a small amount of dilution of TOI-216, which is estimated within the *TESS* aperture to be 0.33%, 0.46%, 0.29%, 0.26%, 0.58% and 0.31% for sectors 1 to 6 respectively (values taken from the *TESS* light curve files) and these are included in our later light curve fits using the prescription of Kipping & Tinetti (2010).

We also highlight that an unresolved companion may reveal itself through centroid shifts during the moments of transit, but all centroid shifts for this star are below 1σ as reported by the *TESS* sector 1-3 cumulative Data Validation (DV) report.

2.4 Light curve detrending

We downloaded sectors 1 to 6 short-cadence (2 minute) data for TIC 55652896 and work with the PDC (Pre-search Data Conditioning) product in what follows (Jenkins et al. 2017). Any bad data flags were removed, and outliers filtered with 5σ clipping against a 20-point moving median. Using the ephemeris and duration for TOI-216.01 and TOI-216.02, we de-weight the in-transit points for the purposes of detrending. The PDC light curve for all six sectors is shown in Figure 1.

We next detrend each transit epoch of each planet independently, using four different algorithms following Teachey & Kipping (2018) - CoFiAM, PoLyAM, local polynomials and a Gaussian Process using a squared exponential kernel. The four light curves are then combined into a single time series

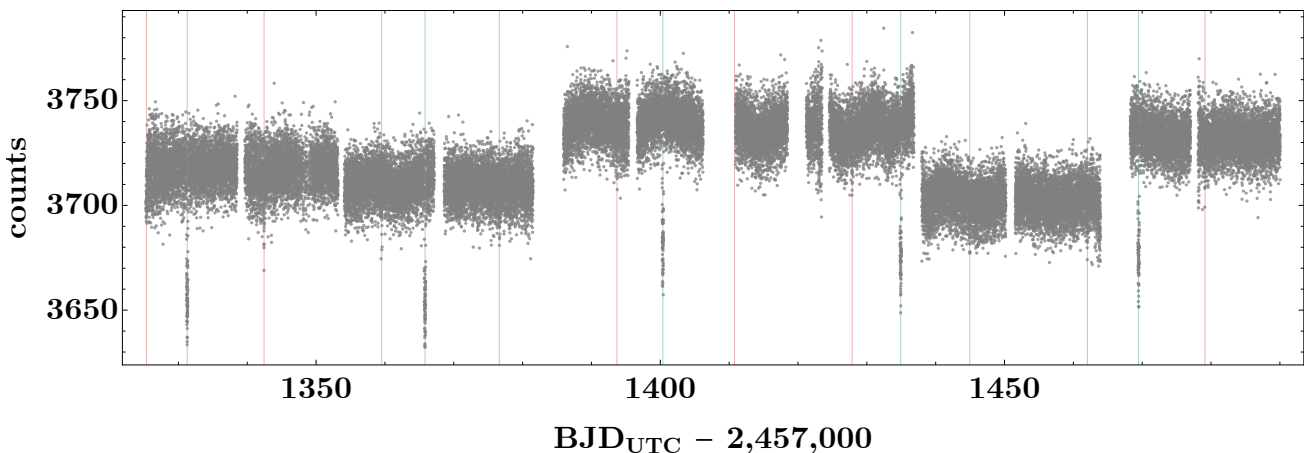


Figure 1. PDC light curve of TIC 55652896 as observed by TESS for sectors 1 to 6. We mark the location of the transits of TOI-216.01 in blue and TOI-216.02 in red.

- a method marginalized light curve - by taking the median at each time stamp and inflating the formal uncertainties by adding the inter-method standard deviation in quadrature. We direct the reader to [Teachey & Kipping \(2018\)](#) for a detailed description of the four algorithms as well as the method marginalization process. The resulting light curves from all four methods, as well as the method marginalized light curves, are made available at [this URL](#).

We find that the inter-method standard deviation is many times smaller than the formal uncertainties, indicating a highly stable detrending. The median formal uncertainty is 2430 ppm but the median inter-method standard deviation is 16 times smaller at 150 ppm. After adding this extra component in quadrature to the formal uncertainties, the error increases by just 0.2%.

3 ANALYSIS

3.1 Light curve model

We initially built light curve models for the system which treated each planetary candidate as orbiting an independent star. It became immediately clear that the transitters displayed strong transit timing variations (TTVs), as can be seen by simple inspection of [Figure 2](#). More detailed analysis of these light curves presented in [Section 3.3](#) reveals strong evidence for anti-correlation - the hallmark of dynamically interacting planets ([Steffen et al. 2013](#)). This is only possible if the two transitters are orbiting the same primary, and thus in our final light curve modeling we decided to treat the objects as sharing a common host star.

This is particularly useful for modeling the inner candidate, TOI-216.02, whose light curve displays a V-shaped morphology consistent with a grazing geometry. Treated as an independent body, V-shaped transits display strong degeneracies between size, impact parameter, limb darkening coefficients and host star density ([Carter et al. 2008](#)). Since the anti-correlated TTVs imply a common host star, and the other transitter is non-grazing, the conditional relationship greatly aids in the inference of a unique light curve solution for TOI-216.02.

Our light curve model is that of the classic [Mandel & Agol \(2002\)](#) quadratic limb darkening code, which is oversampled by a factor of 5 to correct for the slight distortion of finite integration time via the prescription of [Kipping \(2010\)](#). The quadratic limb darkening coefficients are re-parameterized to q_1 & q_2 following [Kipping \(2010\)](#).

Since TTVs are apparent in the light curve ([Figure 2](#)), we allow each transit epoch to have a unique time of transit minimum, τ . In what follows, we also assume both transitters have nearly circular orbits ($e \simeq 0$). If one (or both) were in fact eccentric, the derived stellar density would be erroneous (see [Kipping 2010](#); [Moorhead et al. 2011](#); [Tingley et al. 2011](#); [Dawson & Johnson 2012](#)) by a factor of (marginalizing over argument of periastron, ω):

$$\begin{aligned} \frac{\langle \rho'_* \rangle}{\rho_*} &= \frac{1}{2\pi} \int_{\omega=0}^{2\pi} \frac{(1 + e \sin \omega)^3}{(1 - e^2)^{3/2}} d\omega, \\ &= \frac{1 + \frac{3}{2}e^2}{(1 - e^2)^{3/2}}. \end{aligned} \quad (1)$$

Our later fits (see [Section 3.2](#)) reveal that our light curve derived density is measured to a precision of 6% and thus from [Equation \(1\)](#) one may show that $e < 0.14$ should be expected to lead to a less than 1σ systematic error in the inferred density. As an apparently fairly compact, multiple planet system, we consider this assumption is reasonable on the grounds of dynamical stability, and indeed our later TTV fits favor low eccentricities (see [Section 3.3](#)). Nevertheless, we choose not to use the light curve derived density in any attempt to refine the isochrone modeling from [Section 2.2](#).

3.2 Light curve fits

Our light curve model has a total of 17 free parameters: two ratio-of-radii (p_{inner} & p_{outer}), two impact parameters (b_{inner} & b_{outer}), two limb darkening coefficients (q_1 & q_2), a mean stellar density (ρ_*), six times of transit minimum for the inner transitter ($\tau_{\text{inner},i}$) and four times of transit minimum for the outer transitter ($\tau_{\text{outer},i}$). We assume uniform priors for all parameters except for ρ_* for which we adopt a broad log-uniform prior. All of the priors are listed in [Table 2](#)

Table 2. *Prior probability distributions adopted for the light curve fits. The syntax $\mathcal{U}[a, b]$ denotes a continuous uniform distribution between real values a and b .*

parameter	adopted prior
R_1/R_*	$\mathcal{U}[0, 1]$
R_2/R_*	$\mathcal{U}[0, 1]$
b_1	$\mathcal{U}[0, 2]$
b_2	$\mathcal{U}[0, 2]$
q_1	$\mathcal{U}[0, 1]$
q_2	$\mathcal{U}[0, 1]$
$\log_{10}(\rho_*$ [kg m^{-3}])	$\mathcal{U}[0, 6]$
$\tau_{\text{inner},1}$ [TBJD]	$\mathcal{U}[1324.335632, 1326.335632]$
$\tau_{\text{inner},2}$ [TBJD]	$\mathcal{U}[1341.434774, 1343.434774]$
$\tau_{\text{inner},3}$ [TBJD]	$\mathcal{U}[1358.533916, 1360.533916]$
$\tau_{\text{inner},4}$ [TBJD]	$\mathcal{U}[1375.633058, 1377.633058]$
$\tau_{\text{inner},5}$ [TBJD]	$\mathcal{U}[1392.732200, 1394.732200]$
$\tau_{\text{inner},7}$ [TBJD]	$\mathcal{U}[1426.930484, 1428.930484]$
$\tau_{\text{inner},8}$ [TBJD]	$\mathcal{U}[1444.029626, 1446.029626]$
$\tau_{\text{inner},9}$ [TBJD]	$\mathcal{U}[1461.128768, 1463.128768]$
$\tau_{\text{inner},10}$ [TBJD]	$\mathcal{U}[1478.227910, 1480.227910]$
$\tau_{\text{outer},1}$ [TBJD]	$\mathcal{U}[1330.285130, 1332.285130]$
$\tau_{\text{outer},2}$ [TBJD]	$\mathcal{U}[1364.824472, 1366.824472]$
$\tau_{\text{outer},3}$ [TBJD]	$\mathcal{U}[1399.363814, 1401.363814]$
$\tau_{\text{outer},4}$ [TBJD]	$\mathcal{U}[1433.903156, 1435.903156]$
$\tau_{\text{outer},5}$ [TBJD]	$\mathcal{U}[1468.442498, 1470.442498]$

Table 3. *Medians and one-sigma uncertainties for the ten times of transit minimum in our light curve fit of TOI-216.01 and TOI-216.02.*

parameter	epoch	$BJD_{\text{UTC}} - 2,457,000$
$\tau_{\text{inner},1}$	1	1325.3277 ± 0.0033
$\tau_{\text{inner},2}$	2	1342.4306 ± 0.0027
$\tau_{\text{inner},3}$	3	1359.5398 ± 0.0026
$\tau_{\text{inner},4}$	4	1376.6316 ± 0.0025
$\tau_{\text{inner},5}$	5	1393.7234 ± 0.0029
$\tau_{\text{inner},7}$	7	1427.8784 ± 0.0027
$\tau_{\text{inner},8}$	8	1444.9574 ± 0.0034
$\tau_{\text{inner},9}$	9	1462.0308 ± 0.0034
$\tau_{\text{inner},10}$	10	1479.0951 ± 0.0035
$\tau_{\text{outer},1}$	1	1331.28509 ± 0.00076
$\tau_{\text{outer},2}$	2	1365.82443 ± 0.00074
$\tau_{\text{outer},3}$	3	1400.36868 ± 0.00070
$\tau_{\text{outer},4}$	4	1434.92243 ± 0.00072
$\tau_{\text{outer},5}$	5	1469.47729 ± 0.00098

Fits were conducted using MULTINEST (Feroz & Hobson 2008; Feroz et al. 2009) with 4000 live points², an evidence tolerance of 1.0 and in non-constant efficiency mode. The maximum a-posteriori light curve solution is plotted in Figure 2. We make the full posterior samples available at [this URL](#) but list the credible intervals on the 10 transit times in Table 3 and the other 7 global parameters in Table 5.

² The recommended value is 2000 for posterior estimation (F. Feroz; private communication), but we decided to double this to decrease the chance of a missed mode.

Considering the 7 global parameters, there are two noteworthy conclusions that can be drawn from the results. The first is that the impact parameter of the inner planet is unusually high at $b_{\text{inner}} = 0.957_{-0.022}^{+0.047}$. Given that the ratio-of-radii is measured to be $p_{\text{inner}} = 0.089_{-0.012}^{+0.032}$, then we have $b_{\text{inner}} > 1 - p_{\text{inner}}$ and thus this is a definitively grazing transit. Such transits are rare and have been hypothesized to be powerful probes of nodal variations (Kipping 2009), and thus TOI-216.02 should be carefully monitored in the future for such changes.

Second, the a-posteriori mean stellar density is found to be $2380_{-140}^{+100} \text{ kg m}^{-3}$. We remind the reader that this was using a log-uniform prior and thus was inferred agnostically. The only assumption in the model is that both transits orbit the same star, which is established from the anti-correlated TTVs, and that the eccentricities are small ($e \lesssim 0.14$), which is reasonable given the system's compactness and multiplicity for orbital stability. This density is consistent with the independently derived value from our earlier isochrone analysis (Section 2.2), which yielded $2090_{-300}^{+270} \text{ kg m}^{-3}$ and thus adds further credence to the hypothesis that both transits are orbiting the target star TIC 55652896, rather than some unresolved companion.

3.3 Transit timing variations

We plot the TTVs in Figure 3, where one can clearly see the strong case for anti-correlation mentioned earlier in this work. This establishes that the transits orbit the same star (Steffen et al. 2013), although this point alone does not establish the planetary nature of the two transits. Critically, their masses could potentially be consistent with a brown dwarf or a late-type star, especially for TOI-216.01 whose radius is similar to Jupiter.

The TTVs may be modeled by considering two masses orbiting a primary with an N-body integrator. Dynamical analysis of the observed transit times was performed with an symplectic N-body integrator code described in Nesvorný et al. (2012). The code was instructed to simultaneously fit all transit times of both transits, using MULTINEST to perform the regression. The integration time step was initially set to 0.6 days, but we also repeated for the final fits moving to a higher resolution of 0.3 days to ensure we recover consistent results - which indeed we do. We also note that the results are consistent to that derived when considering just sectors 1-4, which was done in a previous draft of this paper.

Our dynamical model has 14 parameters: mass ratios M_{inner}/M_* and M_{outer}/M_* , orbital periods P_{inner} and P_{outer} , eccentricities e_{inner} and e_{outer} , longitudes of periapsis ϖ_{inner} and ϖ_{outer} , impact parameters b_{inner} and b_{outer} , difference in nodal longitudes $\Omega_{\text{outer}} - \Omega_{\text{inner}}$, stellar density ρ_* , and reference epochs $\tau_{\text{inner,ref}}$ and $\tau_{\text{outer,ref}}$ between a reference time and the first observed transit of each planet. All orbital elements are given at the reference time $2,457,000 BJD_{\text{UTC}}$ (TBJD).

We used uniform priors for all parameters except for b_{inner} , b_{outer} and ρ_* , since our earlier light curve fits provide strong constraints which can be leveraged here. Since MULTINEST requires simple parametric forms of the priors for the purposes of inverse transform sampling, we approximated the marginal posteriors from our earlier fits such that b_{outer} is uniform between 0 and 0.4, b_{inner} is a Gaus-

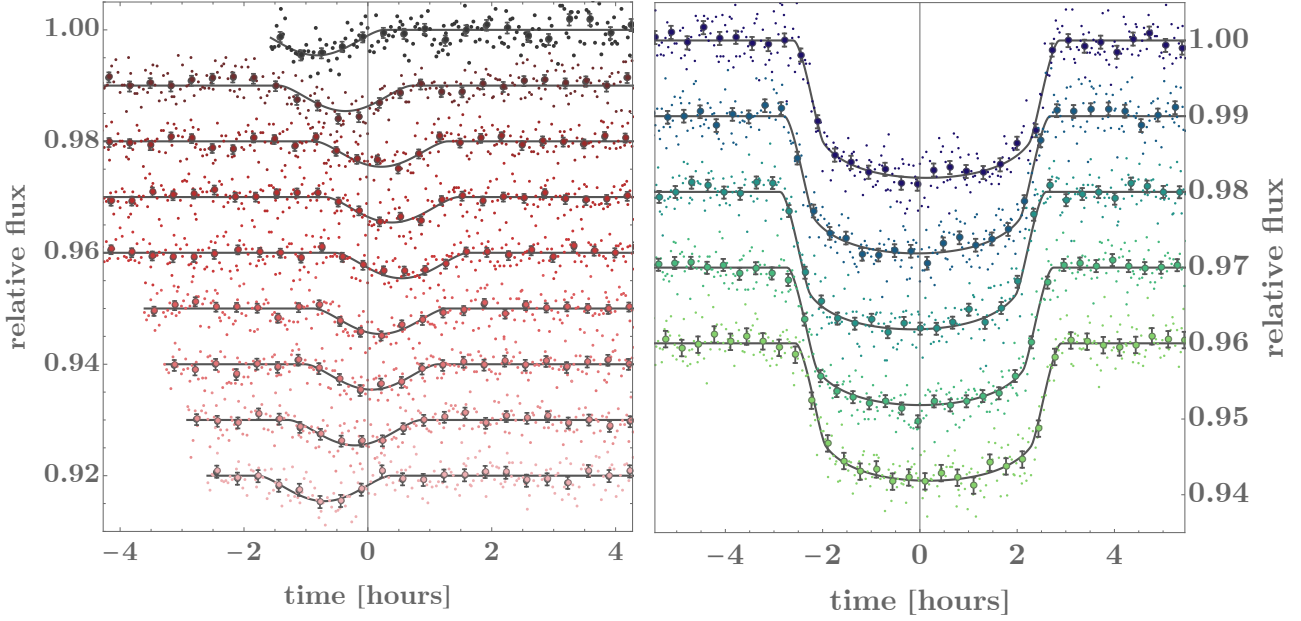


Figure 2. *Left:* The six available transits of TOI-216.02 observed by TESS in sectors 1 to 4 phase folded on the best-fitting linear ephemeris. We bin the data to 20 minute samples and overlay the maximum a-posteriori light curve model. *Right:* Same, but for TOI-216.01, where only four transit are available. In both cases, TTVs are clearly evident.

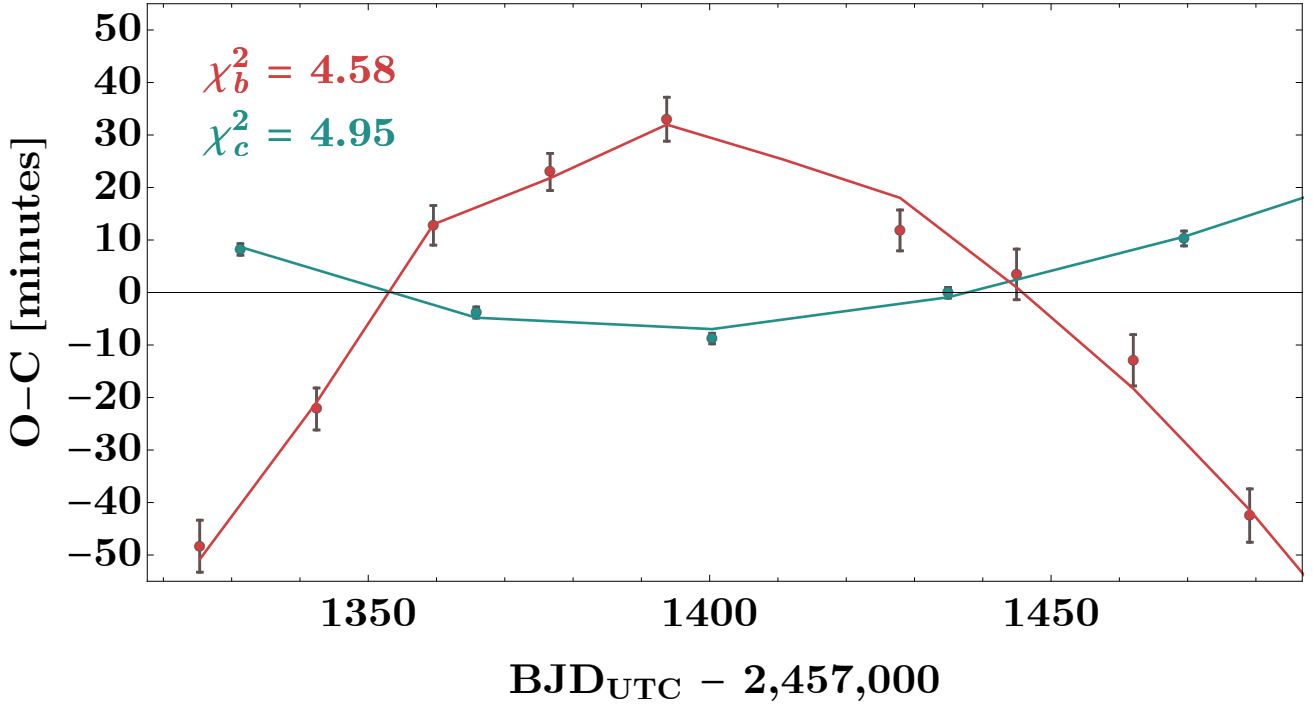


Figure 3. *Observed minus calculated (O-C) transit times of TOI-216.01 (blue) and TOI-216.02 (red). The TTVs are clearly anti-correlated indicating that the transitters orbit the same primary. We overlay the maximum a-posteriori dynamical model with solid lines, described in Section 3.3.*

Table 4. Prior probability distributions adopted for the N -body fits to the transit times. The syntax $\mathcal{U}[a, b]$ denotes a continuous uniform distribution between real values a and b , $\mathcal{N}[a, b]$ is a normal distribution with a mean of a and variance b^2 , and $\mathcal{W}[a, b]$ is a Weibull distribution with scale parameter a and shape parameter b . The upper mass cut-off corresponds to approximately 4.6 Jupiter masses.

parameter	adopted prior
$M_{\text{inner}}/M_{\star}$	$\mathcal{U}[0.0, 0.005]$
$M_{\text{outer}}/M_{\star}$	$\mathcal{U}[0.0, 0.005]$
P_{inner} [days]	$\mathcal{U}[17.0, 17.2]$
P_{outer} [days]	$\mathcal{U}[34.3, 34.7]$
$\tau_{\text{inner.ref}}$ [TBJD]	$\mathcal{U}[1325.231325.43]$
$\tau_{\text{outer.ref}}$ [TBJD]	$\mathcal{U}[1331.181331.38]$
e_{inner}	$\mathcal{U}[0, 0.5]$
e_{outer}	$\mathcal{U}[0, 0.5]$
ϖ_{inner} [rads]	$\mathcal{U}[0, 2\pi]$
ϖ_{outer} [rads]	$\mathcal{U}[0, 2\pi]$
b_{inner}	$\mathcal{N}[0.95, 0.025]$
b_{outer}	$\mathcal{U}[0, 0.4]$
$\Omega_{\text{outer}} - \Omega_{\text{inner}}$ [rads]	$\mathcal{U}[0, 2\pi]$
ρ_{\star} [kg m^{-3}]	$\mathcal{W}[2425, 23]$

sian centered on 0.95 with 0.025 standard deviation and ρ_{\star} is a Weibull prior with shape parameters 22.7 and 2425.1. These priors are listed in Table 4.

The fits converged to a unique solution and the joint posteriors are depicted in Figure 4 for reference. The maximum a-posteriori solution is plotted in Figure 3, which shows how the model is able to fully describe the observed deviations.

Combining the derived mass ratios with the stellar mass derived earlier (see Section 2.2) allows us to measure that $M_{\text{inner}} = 30^{+20}_{-14} M_{\oplus}$ and $M_{\text{outer}} = 200^{+170}_{-100} M_{\oplus}$, which establishes that the masses are far below the deuterium burning limit and these objects may be classified as “planets”. Accordingly, in what follows, we refer to TOI-216.02 as TOI-216b (the inner planet), and TOI-216.01 as TOI-216c (the outer planet).

3.4 Final parameters

To complete our analysis, we combine the fundamental stellar parameters derived earlier (see Section 2.2) with the relative radii (from Section 3.2) and relative masses (from Section 3.3) to calculate physical properties for both planets. Our final planet properties are listed in Table 5.

4 DISCUSSION

We have demonstrated that the *TESS* planetary candidates TOI-216.01 & .02 must orbit the same primary star given their anti-correlated TTVs. The light curve derived stellar density found by fitting both signals yields a value almost precisely equal to the target star’s density from an isochrone analysis, establishing that the objects indeed orbit the target rather than a contaminant. Finally, we have regressed an N -body dynamical model to the observed TTVs to demon-

Table 5. Medians and one-sigma uncertainties for the system parameters of the planets TOI-216b & c. Note that T_{14} is the first-to-fourth contact transit duration, T_{23} is the second-to-third contact transit duration, \tilde{T} is the transit duration from the planet’s center entering to exiting the stellar disk, S denotes insolation and T_{eq} is the equilibrium temperature assuming a zero-albedo blackbody.

parameter	TOI-216b	TOI-216c
P [days]	$17.089^{+0.011}_{-0.015}$	$34.556^{+0.014}_{-0.010}$
τ_0 [BJD _{UTC} - 2,457,000]	$1325.3270^{+0.0026}_{-0.0026}$	$1331.28531^{+0.00068}_{-0.00067}$
b	$0.948^{+0.027}_{-0.017}$	$0.15^{+0.11}_{-0.10}$
a/R_{\star}	$33.25^{+0.46}_{-0.65}$	$53.18^{+0.74}_{-1.04}$
p	$0.0833^{+0.0168}_{-0.0082}$	$0.1235^{+0.0014}_{-0.0014}$
ρ_{\star} [kg m^{-3}]	2380^{+100}_{-140}	2380^{+100}_{-140}
i [°]	$88.364^{+0.042}_{-0.068}$	$89.83^{+0.11}_{-0.12}$
q_1	$0.44^{+0.24}_{-0.18}$	$0.44^{+0.24}_{-0.18}$
q_2	$0.24^{+0.18}_{-0.11}$	$0.24^{+0.18}_{-0.11}$
T_{14} [hours]	$2.062^{+0.068}_{-0.070}$	$5.514^{+0.052}_{-0.047}$
\tilde{T} [hours]	$1.25^{+0.17}_{-0.37}$	$4.890^{+0.054}_{-0.050}$
T_{23} [hours]	0	$4.267^{+0.061}_{-0.067}$
R_p [R_{\oplus}]	$7.69^{+1.62}_{-0.83}$	$11.29^{+0.58}_{-0.42}$
e	$0.132^{+0.059}_{-0.023}$	$0.029^{+0.037}_{-0.020}$
ϖ [°]	193^{+20}_{-35}	275^{+55}_{-113}
Ω [°]	270	270^{+110}_{-110}
M_p [M_{\oplus}]	30^{+20}_{-14}	200^{+170}_{-100}
ρ_p [kg m^{-3}]	340^{+310}_{-180}	760^{+660}_{-380}
a [AU]	$0.1293^{+0.0067}_{-0.0051}$	$0.2069^{+0.0107}_{-0.0082}$
S [S_{\oplus}]	$25.9^{+2.2}_{-1.7}$	$10.1^{+0.85}_{-0.66}$
T_{eq} [K]	628^{+15}_{-11}	497^{+10}_{-8}

strate that the masses of each body are far below the deuterium burning limit making these bona fide “planets”.

The TOI-216 planetary system displays some close similarities to the Kepler-9 system (Holman et al. 2010), but is 1.6 magnitudes brighter in V . In both cases, one finds low-density gas giants in a 2:1 mean motion resonance orbiting a Sun-like star at similar periods (~ 20 d and 40 d). To a lesser degree, the system also resembles KOI-872 (Nesvorný et al. 2012). In both of these cases, the MMR pair of planets are accompanied by a short-period super-Earth and thus it is natural to wonder if perhaps TOI-216 may also be accompanied by a small and currently unresolved terrestrial planet. We ran a box-least squares search (Kovács et al. 2002) for such a signal but find no significant peaks with the available *TESS* data.

The TTVs of TOI-216 are characterized by a super-period as the longitude of conjunctions circulates with a timescale of $\mathcal{O}[10^3]$ days. Although TOI-216 will be monitored throughout the first year of *TESS* observations, the super-period looks likely to exceed this baseline and thus continuous monitoring from the ground in 2020 would greatly benefit the determination of precise orbital elements. With the limited phase coverage available at the time of writing, the masses quoted in this work will surely be refined considerably in the future.

The resonance between the gas giants is consistent with dissipative processes in disk-planet interaction during their presumably inward migration from beyond the snow line (Crida et al. 2008; Havel et al. 2011; Cimerman et al. 2018).

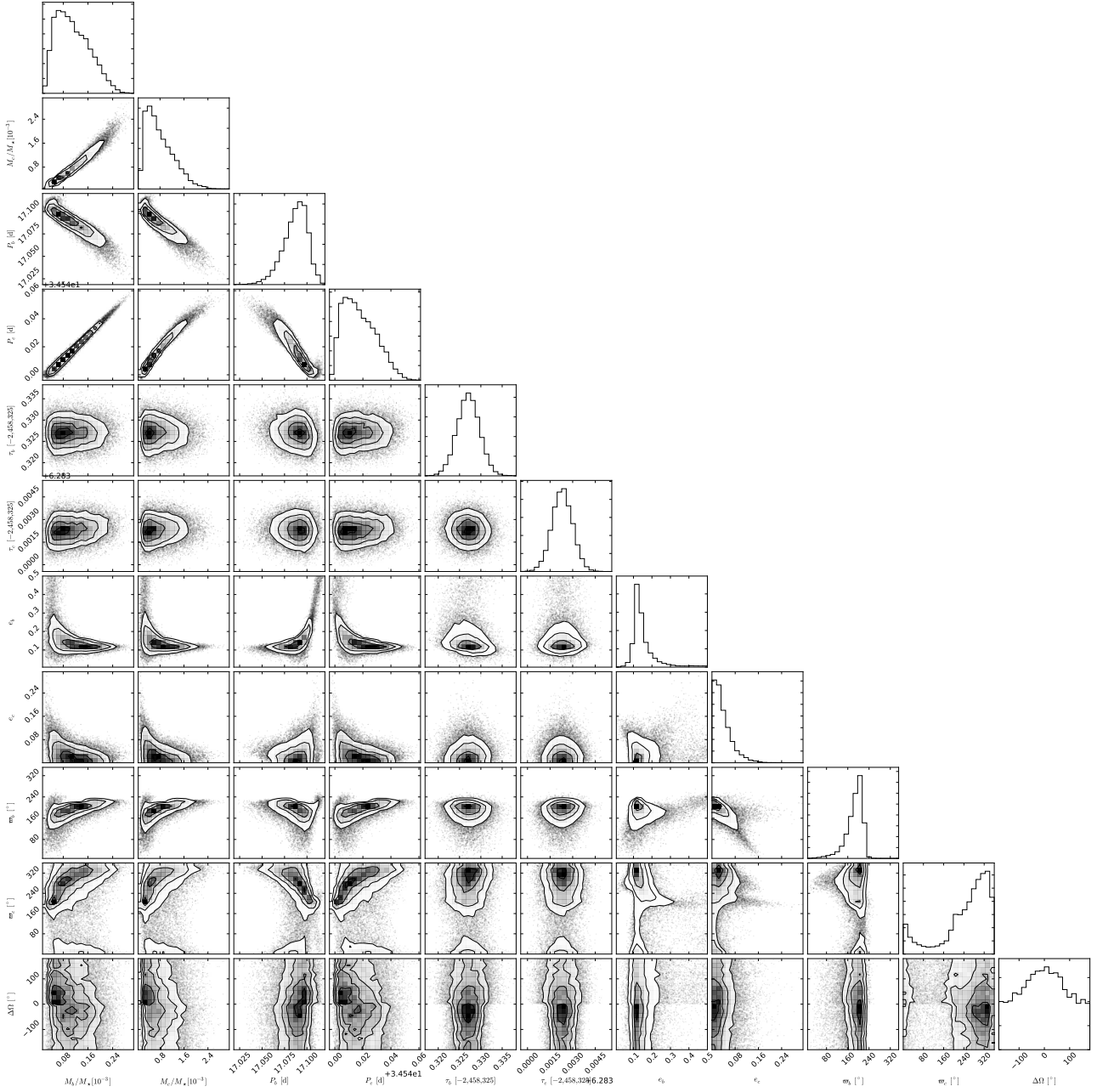


Figure 4. Corner plot of the joint posteriors from our dynamical fits to the TTVs for the TOI-216 system. Since the inferred masses are planetary, we dub the planets “b” and “c” here and in what follows. We omit the terms with informative priors from the earlier light curve fits.

In the Grand Tack hypothesis of the Solar System (Hansen 2009; Walsh et al. 2011), Jupiter is thought to have opened up a gap, migrating slower (type II) than Saturn (type I), which likely failed to fully open a gap. This enabled Saturn to catch up to Jupiter, trapping the pair in resonance when Jupiter was at ~ 1.5 AU, which reversed subsequent migration. In the case of both Kepler-9 and TOI-216, the gas giants have maximum a-posteriori masses similar to Saturn, and thus may have failed to have opened up full gaps, causing them to type I migrate far deeper. As a larger sample of such systems is found in the future, it will be interesting

to test if these giants tend to have sub-Jupiter masses in a statistically significant manner, as would be expected under this hypothesis.

Disk migration is likely a more favorable scenario for the survival of satellite systems around these giants than planet-planet scattering (Gong et al. 2013). Further, the fact that TOI-216 is relatively bright means that follow-up with larger facilities would be well suited to make a search for a satellite system. Similarly, the low-density (high scale height), deep transits and reasonably bright target star would make TOI-216 a potential target for atmospheric characterization

of gas giants in a cooler regime to their hot-Jupiter counterparts. Further, like Kepler-9, the two planets provide an opportunity for differential transit spectroscopy alleviating systematic effects.

ACKNOWLEDGMENTS

DMK is supported by the Alfred P. Sloan Foundation Fellowship. DN's work was supported by the NASA Exoplanet Research Program (XRP). AT & TJ are supported through the NSF Graduate Research Fellowship (DGE 16-44869).

Funding for the TESS mission is provided by NASA's Science Mission directorate. We acknowledge the use of public TESS Alert data from pipelines at the TESS Science Office and at the TESS Science Processing Operations Center. This paper includes data collected by the TESS mission, which are publicly available from the Mikulski Archive for Space Telescopes (MAST).

This work has made use of data from the European Space Agency (ESA) mission Gaia (<https://www.cosmos.esa.int/gaia>), processed by the Gaia Data Processing and Analysis Consortium (DPAC, <https://www.cosmos.esa.int/web/gaia/dpac/consortium>). Funding for the DPAC has been provided by national institutions, in particular the institutions participating in the Gaia Multilateral Agreement. This research has made use of NASA's Astrophysics Data System. This research has made use of the SIMBAD database, operated at CDS, Strasbourg, France. This research has made use of the NASA Exoplanet Archive and the Exoplanet Follow-up Observation Program website, which are operated by the California Institute of Technology, under contract with the National Aeronautics and Space Administration under the Exoplanet Exploration Program.

Facilities: TESS

Software: MULTINEST (Feroz & Hobson 2008; Feroz et al. 2009), isochrones (Morton 2015), Mercury6 (Chambers 1999), corner.py (Foreman-Mackey 2016)

REFERENCES

- Agol, E., Steffen, J., Sari, R. & Clarkson, W., 2005, MNRAS, 359, 567
- Akeson, R. L., Chen, X., Ciardi, D., et al., 2013, PASP, 125, 989
- Bouma, L. G., Winn, J. N., Kosiarek, J., McCullough, P. R., 2017, arXiv e-print:1705.08891
- Carter, J. A., Yee, J. C., Eastman, J., Gaudi, B. S., Winn, J. N., 2008, ApJ, 689, 499
- Chambers, J. E. 1999, MNRAS, 304, 793
- Cimerman, N. P., Kley, W. & Kuiper, R., 2018, A&A, 618, 169
- Crida, A., Sándor, Z., Kley, W., 2008, A&A 483, 325
- Dawson, R. I. & Johnson, J. A., 2012, ApJ, 756, 122
- Deck, K. M. & Agol, E., 2015, ApJ, 802, 116
- Dotter, A., Chaboyer, B., Jevremovic, D., Kostov, V., Baron, E., Ferguson, J. W., 2008, ApJS, 178, 89
- Feroz, F. & Hobson, M. P., 2008, MNRAS, 384, 449
- Feroz, F., Hobson, M. P. & Bridges, M. 2009, MNRAS, 398, 1601
- Ford, E. B., Rowe, J. F., Fabrycky, D. C., et al., 2011, ApJS, 197, 1
- Foreman-Mackey, D., 2016, The Journal of Open Source Software, 24
- Gong, Y.-X., Zhou, J.-L., Xie, J.-W., Wu, X.-M., 2013, ApJ, 769, 14
- Hansen, B. M. S., 2009, ApJ, 703, 1131
- Havel, M., Guillot, T., Valencia, D., Crida, A., 2011, A&A, 531, 3
- Holman, M. J. & Murray, N. W., 2005, Science, 307, 1288
- Holman, M. J., Fabrycky, D. C., Ragozzine, D., et al., 2010, Science, 330, 51.
- Gaia Collaboration, Brown, A. G. A., Vallenari, A., et al., 2018, A&A, 616, 1
- Jenkins, J. M., Tenenbaum, P., Seader, S., et al. 2017, Kepler Science Document, KSCI-19081-002, Edited by Jon M. Jenkins.
- Kipping, D., 2009, MNRAS, 396, 1797
- Kipping, D., 2010, MNRAS, 408, 1758
- Kipping, D., 2010, MNRAS, 407, 301
- Kipping, D. & Tinetti, G., 2010, MNRAS, 407, 2589
- Kipping, D., 2013, MNRAS, 435, 2152
- Kovács, G., Zucker, S. & Mazeh, T., 2002, A&A, 391, 369
- Lithwick, Y., Xie, J. & Wu, Y., 2012, ApJ, 761, 122
- Mandel, K. & Agol, E., 2002, ApJ, 580, 171
- Moorhead, A. V., Ford, E. B., Morehead, R. C., et al. 2011, ApJS, 197, 1
- Morton, T. D., 2015, Astrophysics Source Code Library, record ascl:1503.011
- Nesvorný, D., Kipping, D., Buchhave, L., Bakos, G. Á., Hartman, J. & Schmitt, A., 2012, Science, 336, 1133
- Ricker, G. R., Vandenberg, R., Winn, J., et al., 2016, SPIE, 9904, 2
- Russell, H. N., 1948, "The royal road of eclipses", Harvard Coll. Obs. Monograph, 7, 181
- Stassun, K., Oelkers, R. J., Pepper, J., et al., 2018, AJ, 156, 102
- Steffen, J. H., Fabrycky, D., Eric A., et al., 2013, MNRAS, 428, 1077
- Teachey, A. & Kipping, D., 2018, Science Advances, 4, 1784
- Tingley, B., Bonomo, A. S., & Deeg, H. J., 2011, ApJ, 726, 112
- Walsh, K. J., Morbidelli, A., Raymond, S. N., O'Brien, D. P., Mandell, A. M., 2011, Nature, 475, 206
- Winn, J., 2010, arXiv e-print (arXiv:1001.2010)

This paper has been typeset from a $\text{\TeX}/\text{\LaTeX}$ file prepared by the author.